

An analysis of transverse momentum spectra of various jets produced in high energy collisions

Yang-Ming Tai^{1,2,*}, Pei-Pin Yang^{1,2,†}, Fu-Hu Liu^{1,2,‡}

¹*Institute of Theoretical Physics & State Key Laboratory of Quantum Optics and Quantum Optics Devices, Shanxi University, Taiyuan, Shanxi 030006, People's Republic of China*

²*Collaborative Innovation Center of Extreme Optics, Shanxi University, Taiyuan, Shanxi 030006, People's Republic of China*

Abstract: With the framework of the multi-source thermal model, we analyze the experimental transverse momentum spectra of various jets produced in different collisions at high energies. Two energy sources, a projectile participant quark and a target participant quark, are considered. Each energy source (each participant quark) is assumed to contribute to the transverse momentum distribution to be the TP-like function, i.e. a revised Tsallis–Pareto-type function. The contribution of the two participant quarks to the transverse momentum distribution is then the convolution of two TP-like functions. The model distribution can be used to fit the experimental spectra measured by different collaborations. The related parameters such as the entropy index-related, effective temperature, and revised index are then obtained. The trends of these parameters are useful to understand the characteristic of high energy collisions.

Keywords: Transverse momentum spectra, High-energy jets, TP-like function

PACS: 12.40.Ee, 13.87.Fh, 25.75.Ag, 24.10.Pa

1 Introduction

In central heavy ion (nucleus-nucleus, A-A) collisions at high energy, quark-gluon plasma (QGP) is believed to create possibly [1, 2, 3], because the environment of high temperature and density is formed. After the formation, QGP experiences the process of hadronization and then produces lots of final-state particles. Meanwhile, at the early stage of collisions, some products such as various jets are produced and interact subsequently with QGP. Because of the interactions between jets and QGP, jets lost their energies when they go through QGP region. Not only lots of identified particles but also various jets can be measured in experiments at high energies. Indeed, in the abundant data on high energy collisions, the data on various jets are one of the most important constituents. We are interested in analyzing the experimental transverse momentum (p_T) spectra of various jets, because they can reflect some information of early collisions of participant quarks or partons.

Generally, the p_T spectra of various jets are wider than those of identified particles. In fact, both the p_T spectra of various jets and identified particles cover a wide p_T range. Even if for the later, one may divide the p_T range into low- and high- p_T regions. It is expected that the spectra in low- p_T region are contributed by the soft excitation process, while the spectra in high- p_T region are contributed by the hard scattering process. In some cases, the spectra in low- and high- p_T regions are still complex. One may divide further the low- and high- p_T regions into very low- and low- p_T regions as well as high- and very high- p_T regions respectively. It is expected that the spectra in different p_T regions can be analyzed by different functions. This means that one needs two-component or even four-component function to fit the wide p_T spectra.

It is known that perturbative Quantum Chromodynamics (pQCD) successfully describes the processes which involve large momentum transfers. In particular for proton-proton (p-p) collisions, multi-jet production

*E-mail: taiyangming6@qq.com

†E-mail: yangpeipin@qq.com; peipinyangshanxi@163.com

‡Corresponding author. E-mail: fuhuliu@163.com; fuhuliu@sxu.edu.cn

at high- p_T is well described if initial- and final-state radiations are considered (see e.g. ref. [4]). In addition, multi-parton interactions may play a role at low- p_T [5]. However, pQCD is very complex, which limits its wider applications in high energy proton-nucleus (p-A) and A-A collisions. We hope to use an alternative and thermal-like or statistical method to describe uniformly the spectra of various jets and identified particles in both low- and high- p_T regions in p-p, p-A, and A-A collisions at high energies. As the first step and as an example, we consider the two-component function.

There are two methods to superpose the two components in a function [6, 7, 8]. The first method uses a weighted sum for the two components and there are correlations between the parameters of the two components, though the point of linkage is smooth. The second method uses a step function to link the two components [8] and there is a non-smooth linkage between the two components, though the parameters are uncorrelative. It is imaginable that more issues will appear if we consider four components in a function. Although the two-component function is widely used in literature, it is not an ideal treatment method, not to mention the four-component function. We hope to use a method to treat the two or four components uniformly. Even a single component function is used to fit the spectra in wide p_T range.

Fortunately, to search for the single component function for the spectra in wide p_T range is possible, because the similarity, universality, or common law is existent in high energy collisions [9, 10, 11, 12, 13, 14, 15]. To search for the single component function, we have tested many potential functions. Finally, we have found that the convolution of two or more revised Tsallis–Pareto-type functions [16, 17] is a suitable choice. For the purpose of doing a convenient description, we call the revised Tsallis–Pareto-type function the TP-like function in our recent work [17] and this paper. In fact, the Tsallis–Pareto-type function is more proper to restrict only to a Tsallis distribution, once one essentially uses the non-extensive statistical mechanics [18]. Because the Tsallis distribution has more than one forms of expression, the term of Tsallis–Pareto-type function is used in our work to mention the concrete form.

The application of the convolution of two or more functions is a general treatment method with the framework of the multi-source thermal model [7], where the considered distributions are assumed from the contri-

butions of two or more energy sources. The considered distributions include at least the multiplicity, transverse energy, and transverse momentum (transverse mass) distributions. At least two energy sources are considered in the collisions. Three or more energy sources are not excluded, if the two energy sources are not enough to fit the spectra. The concrete number of energy sources is determined by the quality of fits and the scenario of physics. This fit methodology is suitable and unified for the analyses of spectra in different rapidity intervals, centrality classes, and collision systems.

In this paper, in the framework of the multi-source thermal model, we assume that a projectile participant quark and a target participant quark take part in the production of various jets, and they contribute to the p_T distribution to be the TP-like function [16, 17]. Then, we may use the convolution of two TP-like functions to fit the experimental p_T spectra of various jets. The related data quoted in this paper are from proton-(anti)proton (p-p(\bar{p})), deuteron-gold (d-Au), gold-gold (Au-Au), proton-lead (p-Pb), and lead-lead (Pb-Pb) collisions, with different selection conditions, over a center-of-mass energy ($\sqrt{s_{NN}}$, or simplified as \sqrt{s} for p-p(\bar{p}) collisions) range from 0.2 to 13 TeV.

The remainder of this paper is structured in the following. The formalism and method are described in Section 2. The results and discussion are given in Section 3. Finally, we give the summary and conclusions in Section 4.

2 The formalism and method

According to ref. [16], the Tsallis–Pareto-type function which describes empirically the p_T spectra of particles with rest mass m_0 can be given by

$$f_{p_T}(p_T) = C p_T \left(1 + \frac{\sqrt{p_T^2 + m_0^2} - m_0}{nT} \right)^{-n} \quad (1)$$

which is a probability density function and C is the normalization constant because $\int_0^\infty f_{p_T}(p_T) dp_T = 1$. In Eq. (1), as an entropy index-related parameter, n is related to the entropy index q because $n = 1/(q - 1)$. Generally, $q = 1$ or $n = \infty$ means an equilibrium state. If q is close to 1 or n is large enough, the system is close to an equilibrium state. The free parameter T in Eq. (1) is an effective temperature that describes the excitation and expansion degree of the emission source for particles. We call T the effective temperature because both

the contributions of random thermal motion and flow effect are included.

Equation (1) is not flexible enough in the description of p_T spectra of particles, in particular for the spectra in low- p_T region. Empirically, Eq. (1) can be revised artificially by adding a revised index a_0 that is non-dimensional as the power index of p_T . Then, we have the TP-like function to be [17]

$$f_{p_T}(p_T) = Cp_T^{a_0} \left(1 + \frac{\sqrt{p_T^2 + m_0^2} - m_0}{nT} \right)^{-n}, \quad (2)$$

where C is the normalization constant which is different from that in Eq. (1). For the purpose of convenience, two normalization constants in Eqs. (1) and (2) are represented by the same symbol C , though they may be different. Although one more parameter is introduced, Eq. (2) is more accurate than Eq. (1). In particular, we can obtain Eq. (1) from Eq. (2) if we use $a_0 = 1$.

With the framework of the multi-source thermal model [7], we assume that many quarks or partons take part in the collisions. Each quark or parton is regarded as an energy source. For a given particle or jet, two quarks, i.e. a projectile participant (the first) quark and a target participant (the second) quark, play main role in the production process. Other quarks that take part in the interactions with weak contributions can be neglected. For the two main quarks, the contribution amount or portion (p_{ti}) of each quark to p_T is assumed to obey the TP-like function, where $i = 1$ and 2 are for the first and second quarks respectively. The TP-like function obeyed by p_{ti} is [17]

$$f_i(p_{ti}) = C_i p_{ti}^{a_0} \left(1 + \frac{\sqrt{p_{ti}^2 + m_{0i}^2} - m_{0i}}{nT} \right)^{-n}, \quad (3)$$

where m_{0i} is empirically the constituent mass of the i -th participant quark.

The total amount contributed by the two quarks is the convolution of two TP-like functions. That is [17]

$$f_{p_T}(p_T) = \int_0^{p_T} f_1(p_{t1}) f_2(p_T - p_{t1}) dp_{t1} \quad (4)$$

or

$$f_{p_T}(p_T) = \int_0^{p_T} f_2(p_{t2}) f_1(p_T - p_{t2}) dp_{t2}, \quad (5)$$

where the functions f_1 and f_2 are given by Eq. (3) for various jets which are produced by different collisions which are listed in the table in the next section. In

most cases, the convolution of two TP-like functions is suitable for the spectra of various jets. Correspondingly, two heavy flavor quarks such as $c + \bar{c}$, $b + \bar{b}$, or $t + \bar{t}$ should be considered due to more effective energy being needed. For two light flavor quarks such as $u + \bar{u}$, $d + \bar{d}$, or $s + \bar{s}$, we do not need to consider them due to too less effective energy for the production of various jets.

The method of the convolution of three TP-like functions is similar to that of two TP-like functions. Firstly, we may obtain the convolution $f_{12}(p_{t12})$ of the first two TP-like functions $f_1(p_{t1})$ and $f_2(p_{t2})$. Secondly, we may obtain the convolution $f_{p_T}(p_T)$ of $f_{12}(p_{t12})$ and $f_3(p_{t3})$. Alternatively, we may obtain firstly the convolution $f_{23}(p_{t23})$ of the last two TP-like functions $f_2(p_{t2})$ and $f_3(p_{t3})$, and then we may obtain the convolution $f_{p_T}(p_T)$ of $f_1(p_{t1})$ and $f_{23}(p_{t23})$. The same idea can be used for the convolution of more than three TP-like functions. At present, the convolution of a projectile participant quark and a target participant quark is enough to fit the spectra of p_T of various jets. Temporarily, we do not need to consider the convolution of three or more participant quarks.

Because of the introduction of a_0 , Eq. (2) is more accurate and flexible than Eq. (1). By using a_0 , the spectra in very low- p_T region can be described reasonable. With the framework of the multi-source thermal model, the method of the convolution of two or more probability density functions is applicable for not only the spectra of p_T but also the spectra of multiplicity and transverse energy. In our analysis, the free parameters are n , T , and a_0 . The normalization constant is a parameter, but not a free parameter. The convolution does not introduce new free parameters, but the source number from the collision picture. In the method, to search for the probability density function contributed by a single participant or contributor or source is a key issue. This participant or contributor or source can be quark if we study the spectra of particles, or nucleon if we study the spectra of nuclear fragments.

3 Results and discussion

3.1 Comparison with data

Figure 1 shows the transverse momentum p_T spectra of different jets produced in (a) p-p, (b) d-Au, and (c) Au-Au collisions with mid-pseudorapidity (mid- η , $|\eta| < 0.5$ for Figures 1(a) and 1(c) and $|\eta| < 0.55$ for Fig-

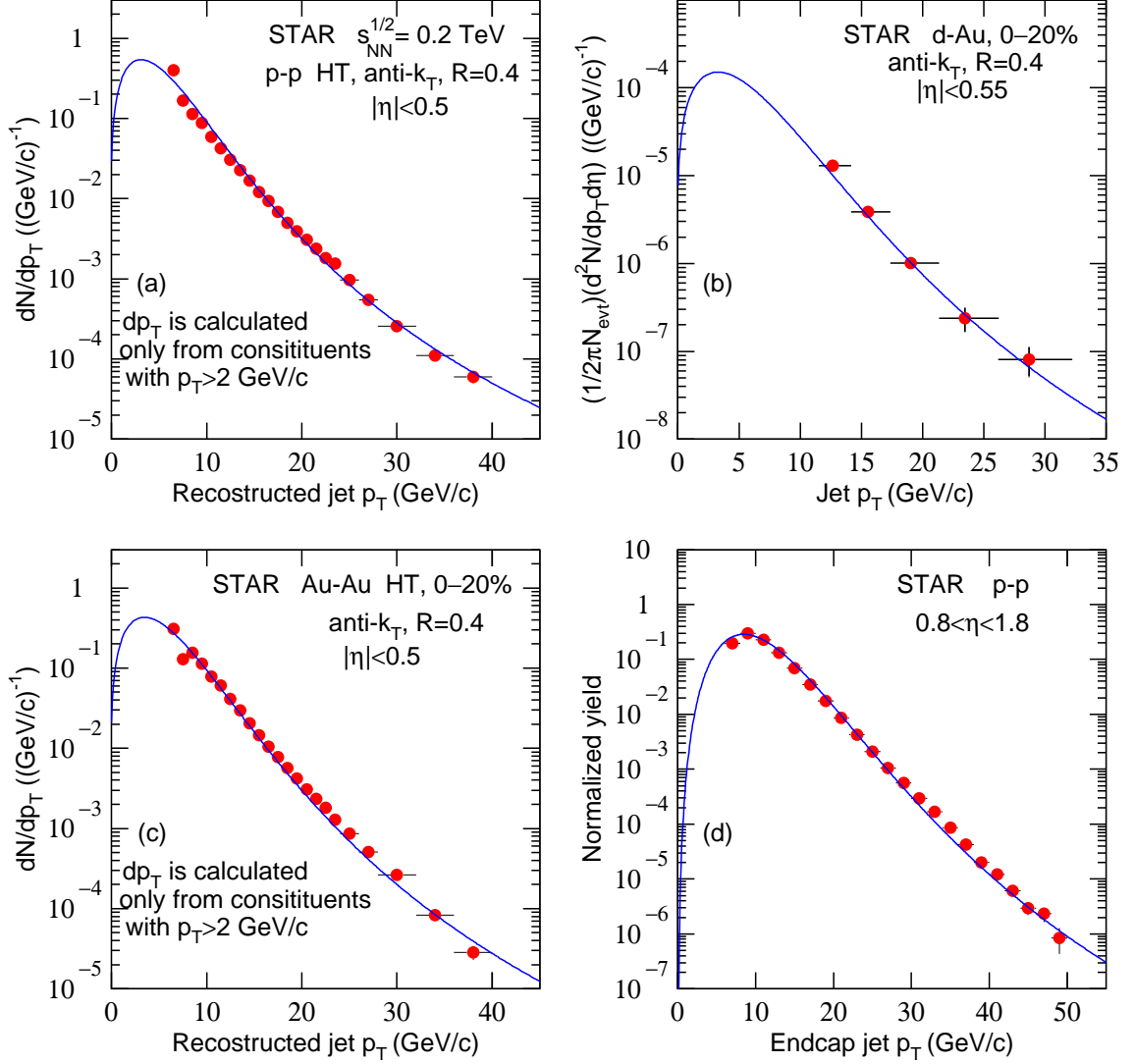


Figure 1. Transverse momentum spectra of different jets produced in (a) p-p, (b) d-Au, and (c) Au-Au collisions with mid- η ($|\eta| < 0.5$ or 0.55), as well as in (d) p-p collisions with non-mid- η ($0.8 < \eta < 1.8$) at $\sqrt{s_{NN}} = 0.2$ TeV. The symbols are cited from the experimental data measured by the STAR Collaboration [19, 20, 21] and the curves are our fitted results with Eq. (4).

ure 1(b)), as well as in (d) p-p collisions with non-mid- η ($0.8 < \eta < 1.8$) at $\sqrt{s_{NN}} = 0.2$ TeV, where N and N_{evt} denote the numbers of jets and events respectively. The symbols are cited from the experimental data measured by the STAR Collaboration [19, 20, 21]. In Figures 1(a) and 1(c), the high tower (HT) trigger jets were selected. In Figure 1(a)–(c), the jet events were selected using a cone radius ($R = 0.4$) and anti- k_T algorithm [22], where k_T denotes the transverse momentum. In Figures 1(b) and 1(c), the data of d-Au and Au-Au collisions were measured in 0–20% centrality class. In the figure, the curves are our fitted results with Eq. (4). In the fit pro-

cess, two participant top quarks with constituent mass of $174 \text{ GeV}/c^2$ for each one are considered. The values of free parameters (n , T , and a_0), normalization constant (N_0), χ^2 , and number of degree of freedom (ndof) are listed in Table 1 in which the parameter trend will be analyzed and discussed in subsection 3.2. One can see that the p_T spectra of different jets are shown to obey approximately the convolution of two TP-like functions. The values of mean excitation and expansion degree (defined by the effective temperature parameter T) seem to not related to the size of collision system in the error range.

Table 1. Values of n , T , a_0 , N_0 (σ_0), χ^2 , and ndof corresponding to the curves in Figures 1–9, where σ_0 is only for Figure 2(a).

Figure and type	Collision	n	T (GeV)	a_0	N_0 [σ_0 (mb)]	χ^2 /ndof
Figure 1(a), p-p, $ \eta < 0.5$	$t + \bar{t}$	2.80 ± 0.12	0.032 ± 0.008	0.00 ± 0.01	3.499 ± 0.002	225/19
Figure 1(b), d-Au, $ \eta < 0.55$	$t + \bar{t}$	3.20 ± 0.02	0.036 ± 0.008	0.00 ± 0.01	0.007 ± 0.001	5/1
Figure 1(c), Au-Au, $ \eta < 0.5$	$t + \bar{t}$	3.20 ± 0.05	0.040 ± 0.009	0.00 ± 0.05	2.999 ± 0.002	249/19
Figure 1(d), p-p, $0.8 < \eta < 1.8$	$t + \bar{t}$	6.00 ± 0.05	0.045 ± 0.001	1.50 ± 0.01	2.499 ± 0.002	195/18
Figure 2(a), p-Pb, 0–20%	$t + \bar{t}$	3.00 ± 0.01	0.130 ± 0.002	1.00 ± 0.02	0.999 ± 0.001	18/4
Figure 2(a), p-Pb, 20–40%	$t + \bar{t}$	3.00 ± 0.02	0.130 ± 0.001	1.00 ± 0.02	0.699 ± 0.002	11/3
Figure 2(a), p-Pb, 40–60%	$t + \bar{t}$	3.00 ± 0.01	0.130 ± 0.003	1.00 ± 0.02	0.499 ± 0.001	12/2
Figure 2(a), p-Pb, 60–80%	$t + \bar{t}$	3.00 ± 0.03	0.130 ± 0.001	1.00 ± 0.02	0.299 ± 0.002	18/2
Figure 2(a), p-Pb, 80–100%	$t + \bar{t}$	3.00 ± 0.05	0.130 ± 0.001	1.00 ± 0.02	0.149 ± 0.002	6/1
Figure 2(b), Pb-Pb, 0–10%	$t + \bar{t}$	3.00 ± 0.11	0.130 ± 0.050	1.00 ± 0.01	$(1.799 \pm 0.001) \times 10^{-5}$	8/5
Figure 2(b), Pb-Pb, 10–30%	$t + \bar{t}$	3.00 ± 0.05	0.140 ± 0.051	1.00 ± 0.01	$(2.299 \pm 0.001) \times 10^{-5}$	3/5
Figure 2(b), Pb-Pb, 30–50%	$t + \bar{t}$	3.00 ± 0.21	0.150 ± 0.052	1.00 ± 0.01	$(2.999 \pm 0.001) \times 10^{-5}$	4/4
Figure 2(b), Pb-Pb, 50–80%	$t + \bar{t}$	3.00 ± 0.31	0.150 ± 0.051	1.00 ± 0.01	$(3.999 \pm 0.002) \times 10^{-5}$	7/3
Figure 3(a), p- \bar{p} , $Z \rightarrow \mu\mu$	$t + \bar{t}$	2.10 ± 0.02	1.150 ± 0.091	-0.45 ± 0.01	259969.508 ± 2.200	106/31
Figure 3(b), p- \bar{p} , $Z \rightarrow ee$	$t + \bar{t}$	2.05 ± 0.05	1.200 ± 0.092	-0.45 ± 0.01	239964.205 ± 2.522	104/31
Figure 3(c), p-p, lepton+jet	$t + \bar{t}$	5.00 ± 0.55	13.000 ± 0.853	-0.48 ± 0.01	199762.511 ± 11.050	257/18
Figure 3(c), p-p, dilepton+jet	$t + \bar{t}$	5.00 ± 0.80	12.000 ± 0.852	-0.48 ± 0.01	51954.412 ± 2.502	201/19
Figure 3(d), p-p, lepton+ b -jet	$b + \bar{b}$	10.00 ± 1.50	12.000 ± 0.893	1.00 ± 0.01	19997.136 ± 0.520	133/29
Figure 3(d), p-p, dilepton+ b -jet	$b + \bar{b}$	10.00 ± 1.50	12.000 ± 0.955	1.00 ± 0.01	2599.627 ± 0.223	57/25
Figure 4(a), 7 TeV p-p, $e+b$ -jet	$b + \bar{b}$	16.00 ± 0.03	15.000 ± 1.512	1.00 ± 0.03	13999.407 ± 0.620	345/12
Figure 4(b), 7 TeV p-p, $\mu+b$ -jet	$b + \bar{b}$	16.00 ± 0.05	16.000 ± 1.502	1.00 ± 0.01	14998.827 ± 0.953	230/12
Figure 4(c), 7 TeV p-p, $e+jet$	$t + \bar{t}$	3.40 ± 0.15	3.500 ± 0.550	1.60 ± 0.13	27400.066 ± 0.965	859/20
Figure 4(d), 7 TeV p-p, $\mu+jet$	$t + \bar{t}$	3.50 ± 0.12	3.500 ± 0.521	1.50 ± 0.10	34924.095 ± 0.856	155/20
Figure 4(e), 8 TeV p-p, $e+jet$	$t + \bar{t}$	3.50 ± 0.42	3.000 ± 0.552	1.50 ± 0.01	119830.499 ± 2.505	509/16
Figure 4(f), 8 TeV p-p, $\mu+jet$	$t + \bar{t}$	3.20 ± 0.35	3.000 ± 0.512	1.40 ± 0.05	159633.552 ± 3.254	832/15
Figure 5, leading jet	$t + \bar{t}$	3.00 ± 0.02	3.600 ± 0.195	1.10 ± 0.12	43983.362 ± 2.562	19/4
Figure 5, 2 nd jet	$t + \bar{t}$	3.00 ± 0.02	1.000 ± 0.190	1.70 ± 0.15	41991.806 ± 3.255	20/3
Figure 5, 3 rd jet	$t + \bar{t}$	2.50 ± 0.01	0.600 ± 0.185	1.00 ± 0.14	42998.320 ± 3.235	6/2
Figure 5, 4 th jet	$t + \bar{t}$	2.50 ± 0.01	0.300 ± 0.095	1.00 ± 0.16	29999.717 ± 2.253	8/1
Figure 5, 5 th jet	$t + \bar{t}$	2.50 ± 0.01	0.150 ± 0.090	1.00 ± 0.12	24999.942 ± 1.025	7/0
Figure 6(a), leading b -jet	$b + \bar{b}$	9.00 ± 0.06	13.000 ± 1.506	1.00 ± 0.05	1097.905 ± 0.252	98/20
Figure 6(b), subleading b -jet	$b + \bar{b}$	6.00 ± 0.10	4.800 ± 0.502	1.00 ± 0.03	1498.243 ± 0.586	11/10
Figure 6(c), leading jet	$t + \bar{t}$	2.01 ± 0.15	7.000 ± 0.520	-0.48 ± 0.01	4998.740 ± 1.562	94/14
Figure 6(d), subleading jet	$t + \bar{t}$	2.10 ± 0.22	2.050 ± 0.510	-0.48 ± 0.01	6965.727 ± 0.852	37/14
Figure 7(a), leading light jet	$c + \bar{c}$	5.00 ± 0.18	11.000 ± 1.505	1.00 ± 0.02	5629.301 ± 0.560	147/36
Figure 7(b), subleading light jet	$c + \bar{c}$	5.50 ± 0.12	4.500 ± 0.150	1.00 ± 0.01	11848.861 ± 0.805	89/36
Figure 7(c), leading jet	$t + \bar{t}$	2.50 ± 0.15	5.000 ± 0.502	0.00 ± 0.03	399824.415 ± 5.600	16/32
Figure 7(d), subleading jet	$t + \bar{t}$	2.50 ± 0.17	2.000 ± 0.105	0.00 ± 0.01	499979.349 ± 2.354	28/32
Figure 8(a), small-R $e+jet$	$t + \bar{t}$	70.00 ± 10.10	70.000 ± 15.100	-0.50 ± 0.02	39936.022 ± 0.500	23/16
Figure 8(b), small-R $\mu+jet$	$t + \bar{t}$	70.00 ± 10.05	90.000 ± 15.520	-0.50 ± 0.05	34825.665 ± 0.850	103/16
Figure 8(c), large-R $e+jet$	$t + \bar{t}$	7.00 ± 0.21	25.000 ± 1.510	1.00 ± 0.03	174997.093 ± 1.220	3/15
Figure 8(d), large-R $\mu+jet$	$t + \bar{t}$	7.00 ± 0.20	24.000 ± 1.521	1.00 ± 0.03	174997.733 ± 1.054	3/15
Figure 9(a), leading, Zjj	$t + \bar{t}$	3.00 ± 0.30	3.200 ± 0.201	1.00 ± 0.05	89955.257 ± 1.523	230/11
Figure 9(b), subleading, Zjj	$t + \bar{t}$	3.00 ± 0.30	1.500 ± 0.100	1.00 ± 0.05	99992.944 ± 1.554	40/11
Figure 9(c), leading, pre-fit	$t + \bar{t}$	3.00 ± 0.11	4.800 ± 0.050	1.00 ± 0.02	93136953.879 ± 15.400	191/9
Figure 9(d), fourth, pre-fit	$t + \bar{t}$	3.50 ± 0.10	0.300 ± 0.010	1.00 ± 0.02	11991257.185 ± 15.600	14/6

Figure 2(a) presents the p_T spectra of fast jets produced in p-Pb collisions with different centralities at $\sqrt{s_{NN}} = 5.02$ TeV, where σ on the vertical axis denotes the cross section. The p_T spectra of charged jets produced in Pb-Pb collisions with different centralities at $\sqrt{s_{NN}} = 2.76$ TeV are presented in Figure 2(b), where

N_{coll} on the vertical axis denotes the number of binary nucleon-nucleon collisions. The symbols are cited from the experimental data measured by the ALICE Collaboration [23, 24]. The jet events were selected with a cone radius ($R = 0.2$) and mid- η ($|\eta| < 0.5$). The curves are our fitted results with Eq. (4), in which two par-

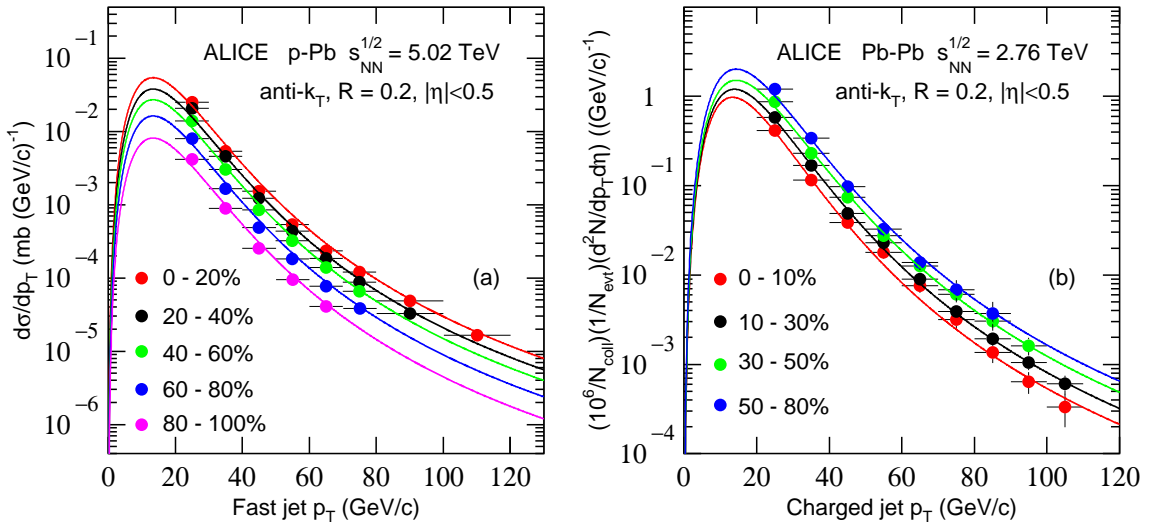


Figure 2. Transverse momentum spectra of (a) fast jets in p-Pb collisions at $\sqrt{s_{NN}} = 5.02$ TeV and (b) charged jets in Pb-Pb collisions at $\sqrt{s_{NN}} = 2.76$ TeV. The different symbols are cited from the experimental data with different centrality classes measured by the ALICE Collaboration [23, 24] and the curves are our fitted results with Eq. (4).

participant top quarks are considered. The values of n , T , a_0 , N_0 , χ^2 , and ndof are listed in Table 1. One can see that the convolution of two TP-like functions describes approximately the experimental data of the mentioned jets. The effective temperature parameter T are the same with changing the centrality percentage in p-Pb collisions. And in Pb-Pb collisions, T increases slightly with the increase of centrality percentage, i.e. T decreases slightly with the increase of centrality itself.

Figure 3(a) (3(b)) presents the p_T spectrum of leading jets corresponding to the $Z \rightarrow \mu\mu$ ($Z \rightarrow ee$) channel in p- \bar{p} collisions at $\sqrt{s} = 1.96$ TeV. Figure 3(c) (3(d)) presents the p_T spectra of jets (b -jets) corresponding to the lepton and dilepton channels in p-p collisions at $\sqrt{s} = 7$ TeV. The symbols are cited from the experimental data measured by the D0 [25, 26], CMS [27], and ATLAS Collaborations [28]. In Figures 3(a) and 3(b), the jet events were selected with a cone radius ($R = 0.5$) and wide η range ($|\eta| < 2.5$). In Figure 3(c) and 3(d), the jet events were selected with $|\eta| < 2.4$ and $|\eta| < 2.5$ respectively. The curves are our fitted results with Eq. (4), in which two participant top quarks are considered for Figures 3(a)–3(c), and two participant bottom quarks with constituent mass of $4.19 \text{ GeV}/c^2$ for each one are considered for Figure 3(d). The values of n , T , a_0 , N_0 , χ^2 , and ndof are listed in Table 1. One can see that the convolution of two TP-like functions provides an approximate description on the data.

The effective temperature parameter T obtained from the spectra with the lepton and dilepton channels are almost the same within the error range.

The p_T spectra of (a)(b) leading b -jets and (c)–(f) leading jets corresponding to the (a)(c)(e) e +jets channel and (b)(d)(f) μ +jets channel in p-p collisions at (a)–(d) $\sqrt{s} = 7$ and (e)(f) 8 TeV are presented in Figure 4. The symbols are cited from the experimental data measured by the ATLAS Collaboration [29, 30, 31]. The jet events were selected with $|\eta| < 2.5$. The curves are our fitted results with Eq. (4), in which two participant bottom quarks are considered for Figures 4(a) and 4(b), and two participant top quarks are considered for Figures 4(c)–4(f). The values of n , T , a_0 , N_0 , χ^2 , and ndof are listed in Table 1. One can see that the fold of two TP-like functions provides an approximate description on the data. The effective temperature parameter T from the e +jets channel and the μ +jets channel are almost the same within the error range.

The reconstructed jet p_T spectra for the leading, 2^{nd} , 3^{rd} , 4^{th} , and 5^{th} order jets in the e +jets channels produced in p-p collisions at $\sqrt{s} = 7$ TeV are shown in Figure 5. The symbols are cited from the experimental data measured by the ATLAS Collaboration [32]. The jet events were selected with a cone radius ($R = 0.4$) and wide η range ($|\eta| < 2.5$). The curves are our fitted results with Eq. (4), in which two participant top quarks are considered. The experimental data are ap-

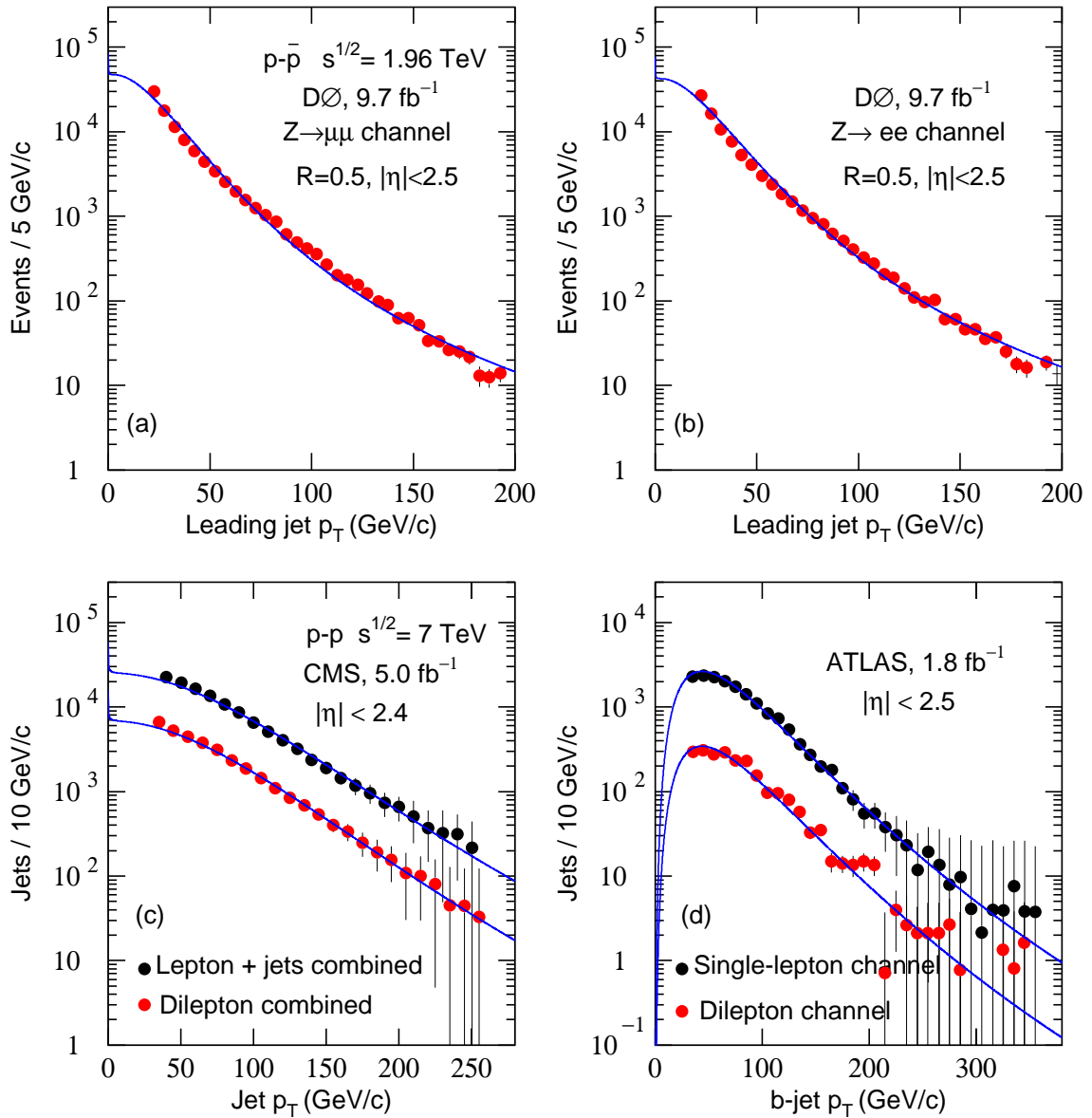


Figure 3. Transverse momentum spectra of (a)(b) leading jets with (a) $Z \rightarrow \mu\mu$ and (b) $Z \rightarrow ee$ in $p\bar{p}$ collisions at $\sqrt{s} = 1.96$ TeV, as well as (c) jets and (d) b -jets in p - p collisions at $\sqrt{s_{NN}} = 7$ TeV with different channels. The symbols are cited from the experimental data measured by the D0 [25, 26], CMS [27], and ATLAS Collaborations [28] and the curves are our fitted results with Eq. (4).

proximately fitted with the convolution of two TP-like functions and the values of related parameters are given in Table 1. One can see that the effective temperature parameter T decreases with the growth of jet order O .

Figure 6 presents the p_T spectra of (a) leading b -jets, (b) subleading b -jets, (c) leading jets, and (d) subleading jets produced in p - p collisions at $\sqrt{s} = 7$ TeV. The symbols are cited from the experimental data measured by the CMS Collaboration [27, 33]. The jet events were selected with (a)(b) $|\eta| < 2.1$ and (c)(d) $|\eta| < 2.4$. The

curves are our fitted results with Eq. (4), in which two participant bottom quarks are considered for Figures 6(a) and 6(b), and two participant top quarks are considered for Figure 6(c) and 6(d). The experimental data are approximately fitted with the convolution of two TP-like functions and the values of related parameters are given in Table 1. The values of T from the spectra of leading jets are much larger than those from the spectra of subleading jets.

Figure 7 displays the p_T spectra of (a) leading light

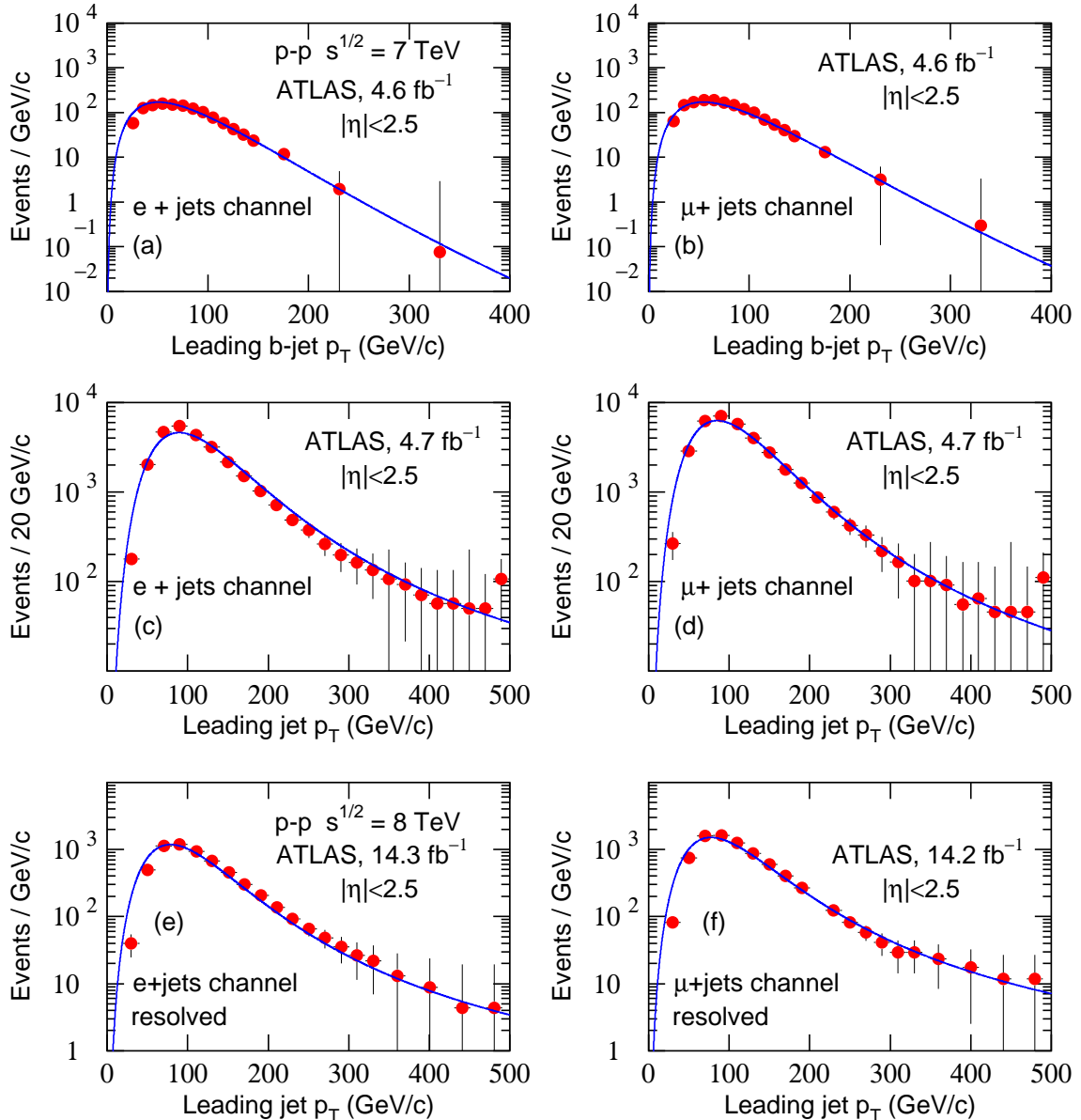


Figure 4. Transverse momentum spectra of (a)(b) leading b -jets and (c)–(f) leading jets corresponding to the (a)(c)(e) e +jets channel and (b)(d)(f) μ +jets channel in p-p collisions at (a)–(d) $\sqrt{s} = 7$ and (e)(f) 8 TeV. The symbols are cited from the experimental data measured by the ATLAS Collaborations [29, 30, 31] and the curves are our fitted results with Eq. (4).

jets, (b) subleading light jets, (c) leading jets, and (d) subleading jets produced in p-p collisions at $\sqrt{s} = 8$ TeV, where N_{obs} denotes the number of observation. The symbols are cited from the experimental data measured by the CMS [34] and ATLAS Collaborations [35]. The jet events were selected with $|\eta| < 2.4$. The curves are our fitted results with Eq. (4), in which two participant charm quarks with constituent mass of 1.27 GeV/ c^2 for each one are considered for Figures 7(a) and 7(b), and two participant top quarks are considered for

Figure 7(c) and 7(d). The experimental data are approximately fitted with the convolution of two TP-like functions and the values of related parameters are given in Table 1. Once more, the values of T from the spectra of leading jets are much larger than those from the spectra of subleading jets.

The p_T spectra of (a)(b) small-R selected and (c)(d) large-R jets corresponding to the (a)(c) e +jets and (b)(d) μ +jets channels produced in p-p collisions at $\sqrt{s} = 13$ TeV are shown in Figure 8. The symbols are

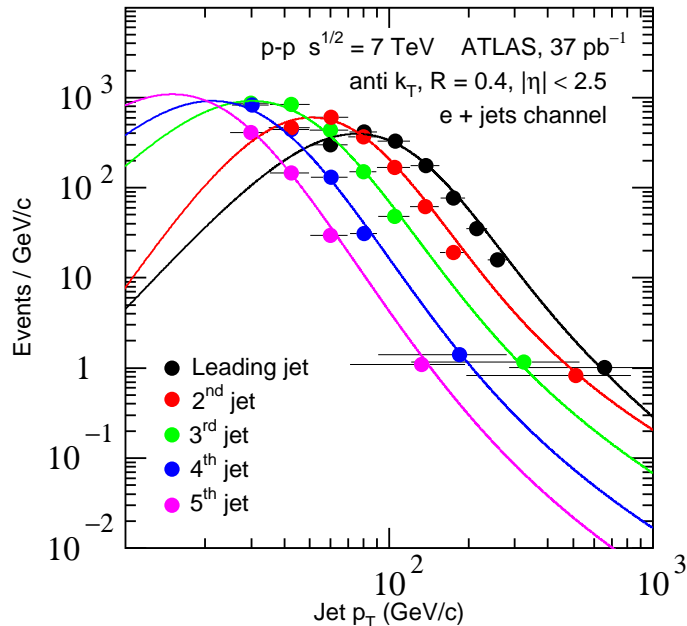


Figure 5. Transverse momentum spectra of reconstructed jets with different orders in p-p collisions at $\sqrt{s} = 7$ TeV. The symbols are cited from the experimental data measured by the ATLAS Collaboration [32] and the curves are our fitted results with Eq. (4).

cited from the experimental data measured by the ATLAS Collaboration [36]. The curves are our fitted results with Eq. (4), in which two participant top quarks are considered. The experimental data are approximately fitted with the convolution of two TP-like functions and the values of related parameters are given in Table 1. One can see that the values of T from the spectra of e +jets and μ +jets channels are almost the same within the error range.

The p_T spectra of (a) the leading jets and (b) the subleading jets in Zjj baseline region as well as (c) the leading jets and (d) the forth jets with pre-fit produced in p-p collisions at $\sqrt{s} = 13$ TeV are presented in Figure 9. The symbols are cited from the experimental data measured by the ATLAS Collaboration [37, 38]. The jet events were selected with $|y| < 2.4$ for Figures 9(a) and 9(b), and $|\eta| < 2.5$ for Figures 9(c) and 9(d). The curves are our fitted results with Eq. (4), in which two participant top quarks are considered. The experimental data are approximately fitted with the convolution of two TP-like functions and the values of related parameters are given in Table 1, in which the normalization is very large due to the fact that it denotes the event number accumulated, but not the cross section or jet number per event. One can see that the values of T from the spectra of the leading jets are much larger than those

from the spectra of the subleading and forth jets.

From the above comparison with data, one can see that the data are approximately fitted with the convolution of two TP-like functions. In most cases, the quality of the fits is acceptable due to appropriate χ^2/ndof . In a few cases, the result of the fits is worthy of further improvement due to large χ^2/ndof . To improve the result, we need more suitable function for the component and/or three or more functions in the convolution. In addition, there are cases in which some parameters do not change but others suffer significant changes, in that sense is not possible to conclude about the characteristics of high energy collisions. Indeed, as an application of the uniform method, more comparisons with data are needed in future. Meanwhile, we hope to improve the result of the fits in future.

3.2 Parameter trend and discussion

Although the comparison with data is not perfect, one can also see some trends in most cases. To show the trends of main parameters, Figure 10(a) presents the relation of the effective temperature T and the centrality percentage C in Pb-Pb collisions at $\sqrt{s_{NN}} = 2.76$ TeV. The symbols represent the values of T obtained from Figure 2 and listed in Table 1. The curve is our fit by

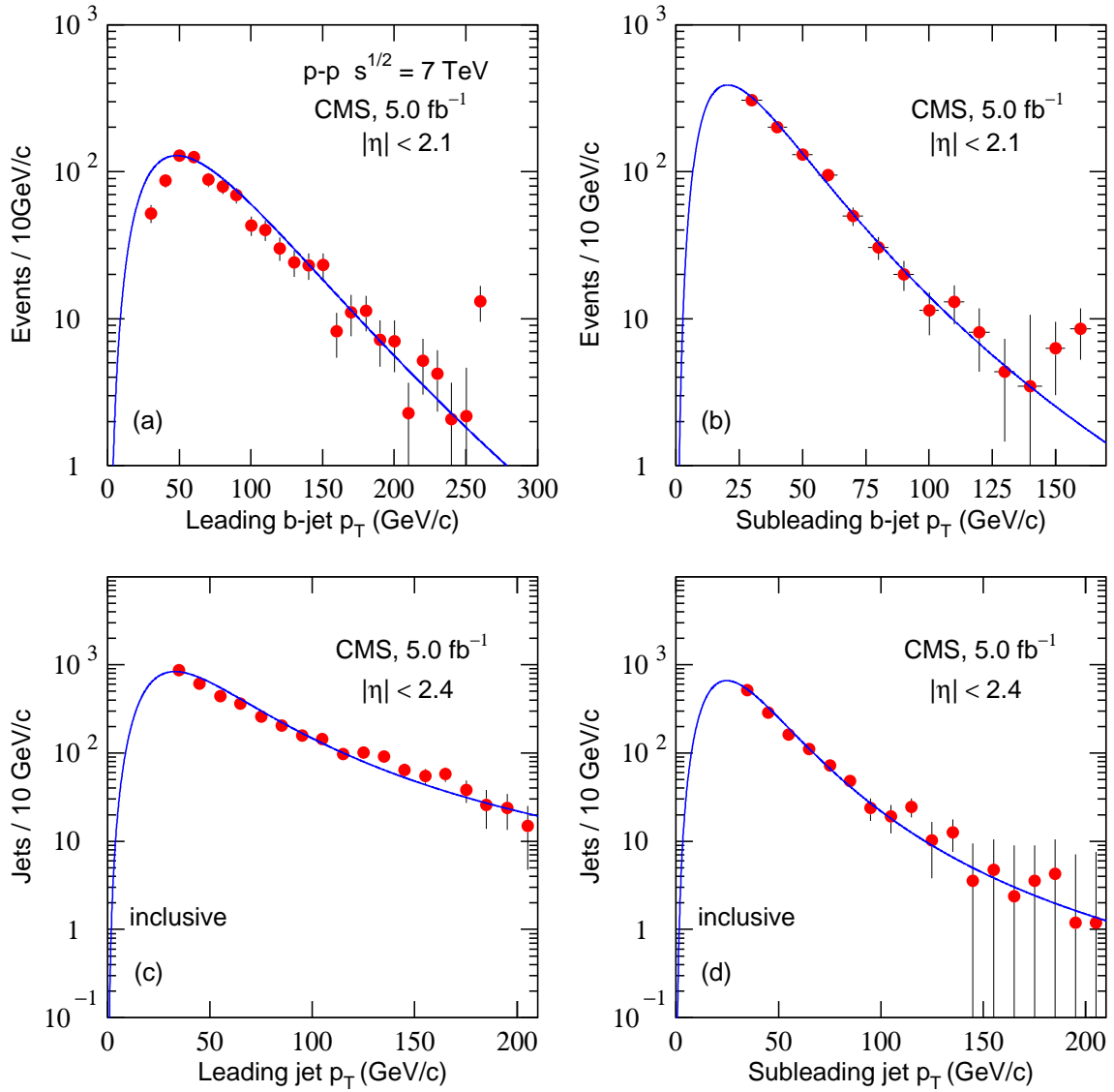


Figure 6. Transverse momentum spectra of (a) leading b -jets, (b) subleading b -jets, (c) leading jets, and (d) subleading jets produced in p-p collisions at $\sqrt{s} = 7$ TeV. The symbols are cited from the experimental data measured by the CMS Collaboration [27, 33] and the curves are our fitted results with Eq. (4).

an exponential function

$$T = (-0.03 \pm 0.01) \exp\left(\frac{-C}{17.00 \pm 2.00}\right) + (0.15 \pm 0.01), \quad (6)$$

in which T and C are in GeV and % respectively. One can see that T increases slightly with the increase of C , or T are almost the same within the error range when C varies. The relation between T and C renders that QGP formed in central Pb-Pb collisions has less influence on the jet transport. Or, in the transport process of jets in QGP in central Pb-Pb collisions, jets lost less energy.

Figure 10(b) presents the relation of the effective temperature T and the jet order O in p-p collisions at $\sqrt{s} = 7$ TeV. The symbols represent the values of T obtained from Figure 5 and listed in Table 1. The curve is our fit by an exponential function

$$T = (11.00 \pm 0.10) \exp\left(\frac{-O}{0.80 \pm 0.01}\right) + (0.20 \pm 0.01), \quad (7)$$

in which T is in GeV. One can see that T decreases with the growth of O . This trend is natural due to the fact that the jet with high order corresponds to the source

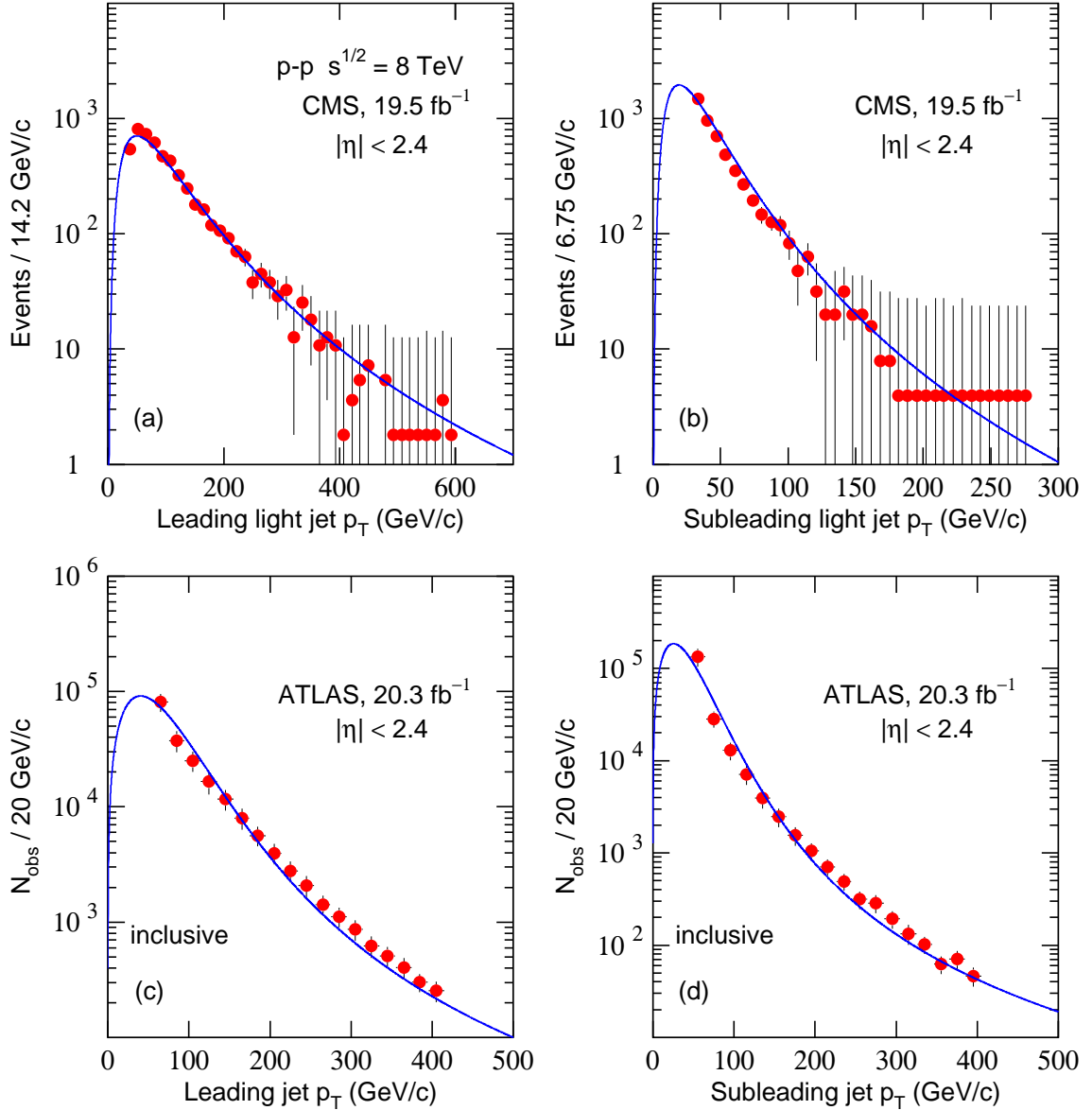


Figure 7. Transverse momentum spectra of (a) leading light jets, (b) subleading light jets, (c) leading jets, and (d) subleading jets produced in p-p collisions at $\sqrt{s} = 8$ TeV. The symbols are cited from the experimental data measured by the CMS [34] and ATLAS Collaborations [35] and the curves are our fitted results with Eq. (4).

with less excitation degree.

Figure 11 shows the relations of the effective temperature T and (a) the size of interacting system, (b) ℓ and di- ℓ channels, (c) $\mu(\mu\mu)$ and $e(ee)$ channels, and (d) leading and sub-leading jets. The symbols represent the values of T obtained from the above figures and listed in Table 1. One can see that T seems to not related to the system size in the error range. This is in agreement with the conclusion from Figure 10(a) in which central collisions correspond to large system and peripheral collisions correspond to small system. In the error range,

different lepton channels show nearly the same effective temperature, which renders nearly the same excitation degree of source. At the same time, the values of T from the spectra of leading jets are much larger than those from the spectra of subleading jets, which is the same as the conclusion from Figure 10(b).

As a parameter determining the curvature in middle- p_T region and the extended range in high- p_T region, n is related to the entropy index q because $n = 1/(q-1)$. In most cases, $q \geq 1.2$ which is not close to 1 because $n \leq 5$ which is not large. This implies that the source of jets

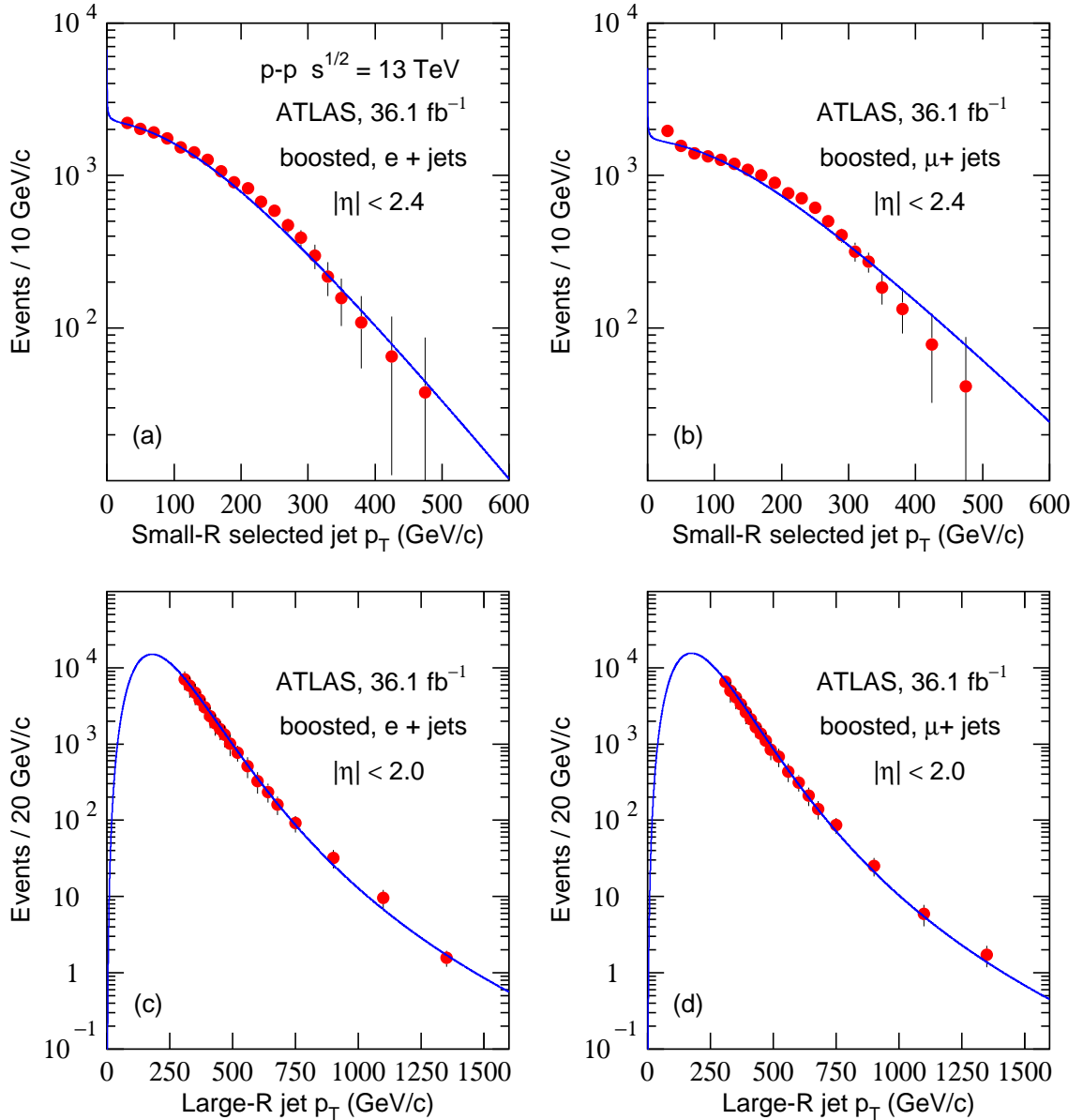


Figure 8. Transverse momentum spectra of (a)(b) small-R selected and (c)(d) large-R jets corresponding to the (a)(c) e +jets and (b)(d) μ +jets channels produced in p-p collisions at $\sqrt{s} = 13$ TeV. The symbols are cited from the experimental data measured by the ATLAS Collaboration [36] and the curves are our fitted results with Eq. (4).

does not stay at the equilibrium state. In a few cases, n is large and q is close to 1. This happens coincidentally, but not implies that the source of jets stay at the equilibrium state. This situation is different from the source of identified particles. Generally, the source of identified particles stays approximately at the equilibrium or local equilibrium state. These non-equilibrium and (local) equilibrium states do not mean a contradiction between the productions of various jets and identified particles. In fact, the two types of products are produced at differ-

ent stages of system evolution. Generally, various jets are produced at the initial stage, and the identified particles are produced at the kinetic freeze-out stage. From the initial to kinetic freeze-out stages, the collision system evolves quickly from non-equilibrium to (local) equilibrium states.

An a parameter determining the slope of the curve in low- p_T region, a_0 is elastic from negative to positive values. A negative a_0 results in a cocked up distribution and a positive a_0 results in a falling distribution.

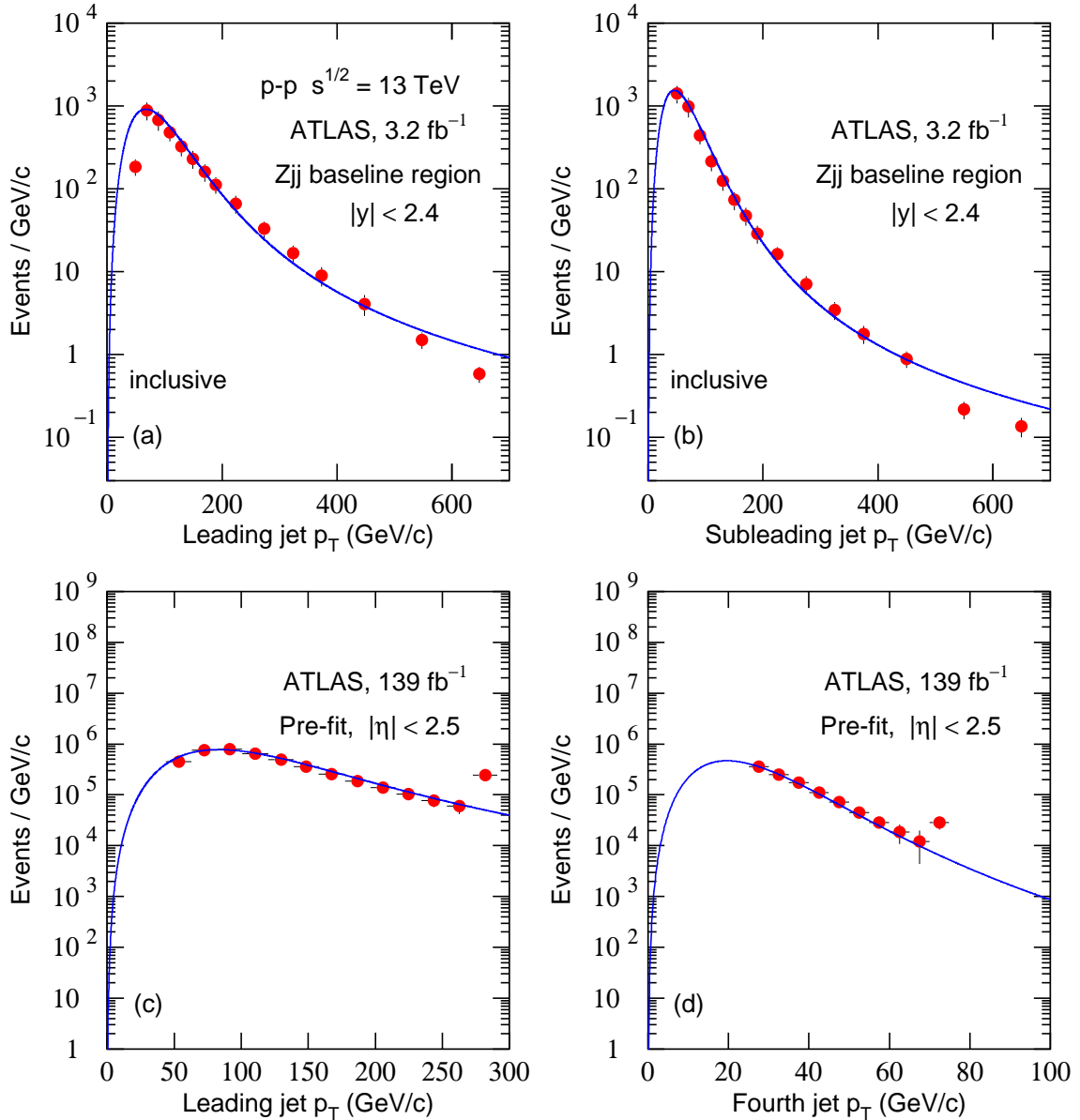


Figure 9. Transverse momentum spectra of (a) the leading jets and (b) the subleading jets in Zjj baseline region as well as (c) the leading jets and (d) the fourth jets with pre-fit produced in p-p collisions at $\sqrt{s} = 13$ TeV. The symbols are cited from the experimental data measured by the ATLAS Collaboration [37, 38] and the curves are our fitted results with Eq. (4).

In many cases, $a_0 \neq 1$ which means that it is necessary introducing a_0 in the Tsallis–Pareto-type function. Due to the introduction of a_0 , the revised Tsallis–Pareto-type function, i.e. the TP-like function becomes more flexible. The convolution of two or more TP-like functions is expected to fit more p_T spectra in high energy collisions. The effective temperature T from the spectra of leading jets is much larger than that from the spectra of subleading jets because the leading jets undergone more violent scattering. However, a_0 parameter

does not change usually with the order of jet because a_0 determines only the spectra at low- p_T . To determine T , the spectra at medium- and high- p_T play main role. Generally, the parameters related to various jets are not associated with the flow because various jets are produced at the initial stage where the flow is not formed. The flow is associated with identified particles which are finally produced at the kinetic freeze-out stage where the flow is formed.

It is accepted that, regarding central A-A collisions

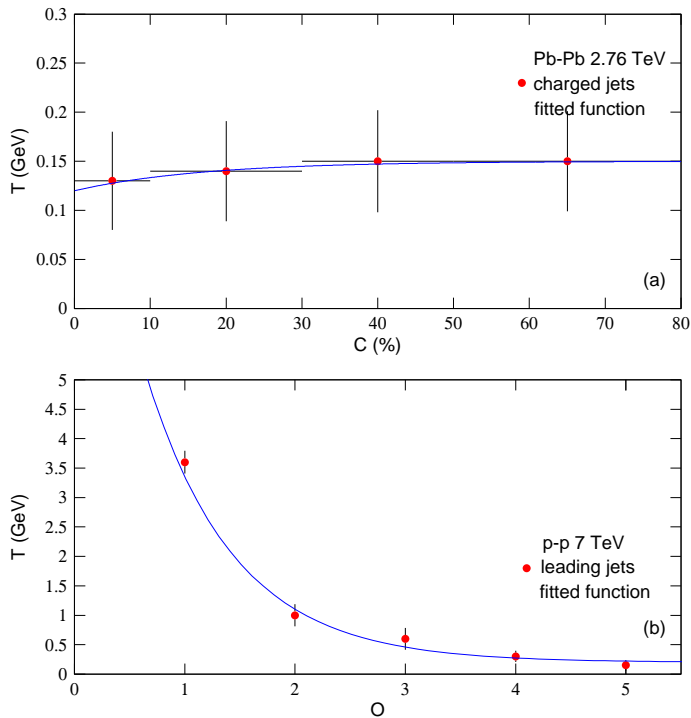


Figure 10. The relations of (a) the effective temperature parameter T and the centrality percentage C in Pb-Pb collisions at $\sqrt{s} = 2.76$ TeV, as well as (b) T and the jet order O in p-p collisions at $\sqrt{s} = 7$ TeV. The symbols represent the values of T obtained from Figures 2 and 5 and listed in Table 1. The curves are our fitted results with Eqs. (6) and (7) respectively.

at high energies, jets lose considerably energy as they propagate through the hot and dense medium [39]. Due to the loss of energy, the p_T spectra are reduced and we obtain seemingly a relative small T and/or large n (small q) comparing with peripheral A-A collisions. However, due to large error, T in A-A collisions also shows a nearly invariant trend. In central p-A collisions, jets do not lose considerably energy and the p_T spectra are not reduced due to similar small participant volume comparing with peripheral p-A collisions. This renders that the main parameters in p-A collisions are independent of centrality, as what appear in A-A collisions. Mostly, the spectra of jets cited from p-A and A-A collisions are not under the same condition, it is hard to compare the parameters directly.

In A-A collisions, the medium effect on the probe of hard process is commonly referred to as jet quenching. The effect has been observed via deviations from a well-calibrated baseline established in the absence of a medium (e.g. in minimum-bias p-p collisions). The generic strategy is illustrated with the nuclear modification factor (R_{AA}), which evaluates the deviation of a single particle inclusive spectra away from the baseline.

R_{AA} is expected to be one in the absence of medium effect. Jet measurements in central A-A collisions at high energies have shown that R_{AA} is p_T dependent and it is smaller than one. For peripheral A-A collisions R_{AA} approaches to unity and it is nearly flat (see e.g. [40]). An analogous analysis in p-A collisions gives a R_{pA} which is consistent to one (see e.g. [23]).

It seems that these features of data on R_{AA} are not captured by the parameters presented in Table 1. For instance, the extracted parameters which characterize the spectral shape (a_0 , T , and n) are the same for central A-A collisions and 0-100% p-A collisions. Probably this is not a surprise because based on the reduced χ^2 , the proposed function seems not describe all the data which are analyzed in the paper. This seems to illustrate that the paper also lacks consistent results. In fact, these opinions cannot be obtained because the parameters from A-A and p-A collisions cannot be compared directly. As we know, in Figure 2, the spectra in A-A and p-A collisions are from different kinds of jets. The same parameters for the two collisions are coincidental due to the similar trends of data quoted.

Before summary and conclusions, we would like to

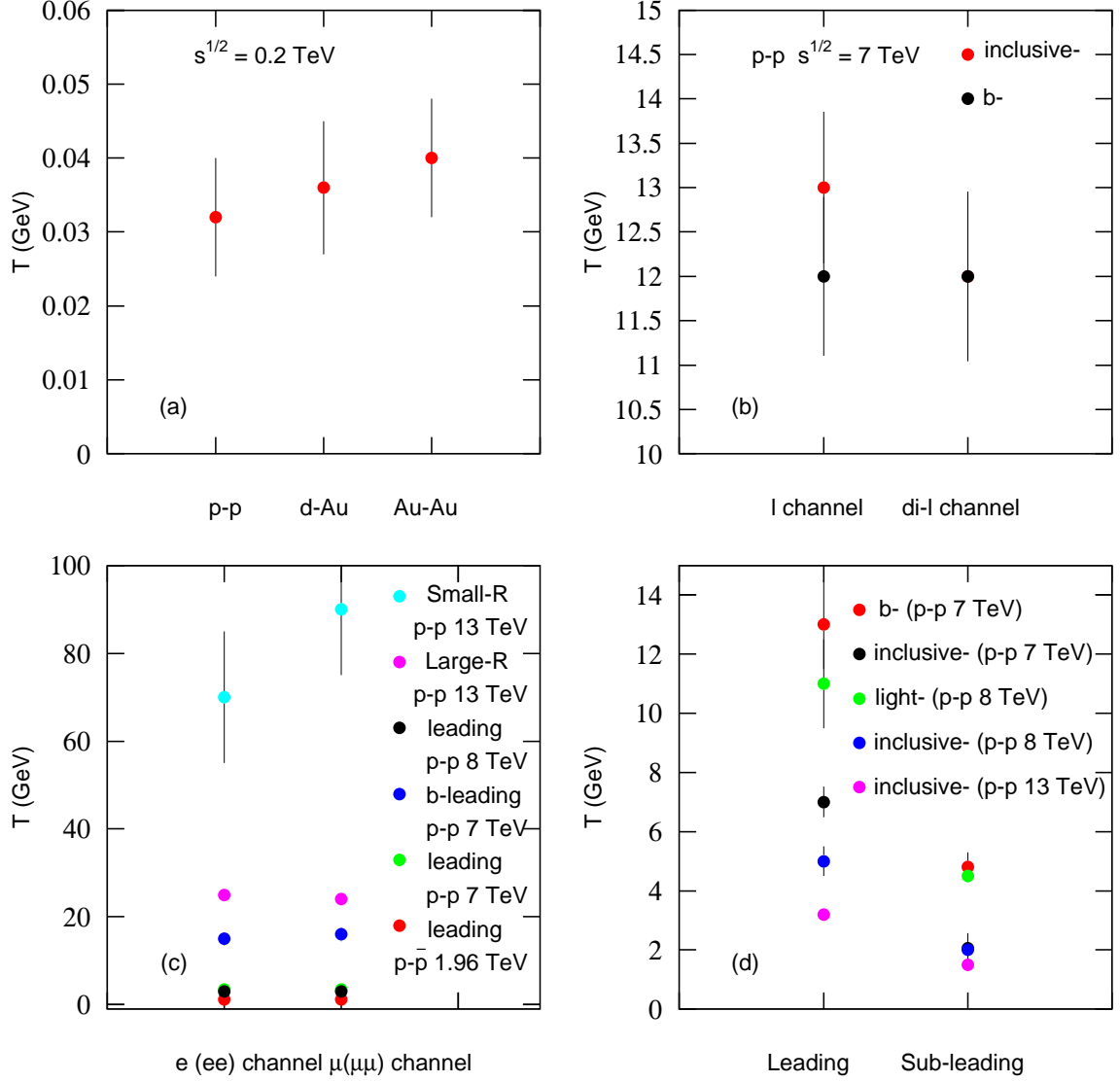


Figure 11. The relations of the effective temperature parameter T and (a) the size of interacting system, (b) the ℓ and di- ℓ channels, (c) the e (ee) and μ ($\mu\mu$) channels, as well as (d) the leading and sub-leading jets. The symbols represent the values of T obtained from various figures and listed in Table 1.

emphasize the functions of parameters. As what we discussed in our recent work [17], the power index a_0 describes flexibly the shapes of spectra at low- p_T . From negative to positive a_0 , the spectra bend from up to down over a p_T range from 0 to 1 GeV/ c . Correspondingly, the spectra at medium- and high- p_T change higher due to the result of normalization. With the increase of T and by fixing a_0 and n , the spectra become wider. Meanwhile, with the increase of n and by fixing a_0 and T , the spectra become narrower. However, the changes with the increases of T and n cannot be offset. Anyhow, the introduction of a_0 makes the TP-like function more

flexible.

We would like to point out that the effective temperature is one of the reported parameters, however, the kinetic freeze-out temperature (T_0) should be more important to disentangle the T_0 and flow. We have been worked on it for identified particles in our previous work [41]. In fact, that paper reports an increase of T_0 with the collision energy, as well as the mass dependence of the T_0 . The present work and our previous work are not contradictory. However, we cannot compare them directly due to different stages of considerations. The identified particles are studied at the stage of kinetic

freeze-out, while various jets are produced at the stage of initial collisions. In addition, different fit functions which correspond to different “thermometers” are used, which also increases the degree of difficulty for direct comparisons.

4 Summary and conclusions

We summarize here our main observations and conclusions.

(a) The transverse momentum p_T spectra of various jets selected in different conditions and produced in different collisions over an energy range from 0.2 to 13 TeV are fitted by the convolution of two TP-like functions, where the TP-like function is a revised Tsallis–Pareto-type function. The experimental data recorded by various collaborations are approximately fitted by the mentioned convolution.

(b) From the fit on the p_T spectra of charged jets produced in Pb-Pb collisions at $\sqrt{s} = 2.76$ TeV with different centrality intervals, we know that the effective temperature T increases slightly with increasing the centrality percentage, or T is almost the same in the error range when the centrality changes. Meanwhile, T from the spectra of jets in p-p, d-Au, and Au-Au collisions at 0.2 TeV does not show the size dependence. This is consistent to the nearly independence of T on centrality.

(c) The values of T from the spectra of leading jets are much larger than those from the spectra of subleading jets due to the leading jets undergone more violent scattering. As expected, T extracted from the reconstructed jets produced in p-p collisions at $\sqrt{s} = 7$ TeV decreases with the growth of the jet order. In addition, T from the lepton and dilepton channels are almost the same, which means that these jets have common property.

(d) The parameter n determines the curvature in middle- p_T region and the extended range in high- p_T region. Meanwhile, n is related to the entropy index q because $n = 1/(q - 1)$. Generally, n is not too large. This means that q is not close to 1 and the source of jets does not stay at the equilibrium state. This is different from the source of identified particles which stays approximately at the equilibrium or local equilibrium state.

(e) The parameter a_0 determines the slope of the curve in low- p_T region. A negative a_0 results in a

cocked up distribution and a positive a_0 results in a falling distribution. Due to the introduction of a_0 in the Tsallis–Pareto-type function, the revised function, i.e. the TP-like function, becomes more flexible. The convolution of two or more TP-like functions is expected to have more applications.

Data Availability

The data used to support the findings of this study are included within the article and are cited at relevant places within the text as references.

Ethical Approval

The authors declare that they are in compliance with ethical standards regarding the content of this paper.

Disclosure

The funding agencies have no role in the design of the study; in the collection, analysis, or interpretation of the data; in the writing of the manuscript; or in the decision to publish the results.

Conflict of Interest

The authors declare that there are no conflicts of interest regarding the publication of this paper.

Acknowledgments

The work of the first author (Y.M.T.) was supported by Shanxi University. The work of the second author (P.P.Y.) was supported by the China Scholarship Council (Chinese Government Scholarship) under Grant No. 202008140170 and the Shanxi Provincial Innovative Foundation for Graduate Education under Grant No. 2019SY053. The work of the third author (F.H.L.) was supported by the National Natural Science Foundation of China under Grant Nos. 11575103 and 11947418, the Scientific and Technological Innovation Programs of Higher Education Institutions in Shanxi (STIP) under Grant No. 201802017, the Shanxi Provincial Natural Science Foundation under Grant No. 201901D111043, and the Fund for Shanxi “1331 Project” Key Subjects Construction.

References

- [1] J. Adams et al. (STAR Collaboration), “Experimental and theoretical challenges in the search for the quark–gluon plasma: The STAR Collaboration’s critical as-

- assessment of the evidence from RHIC collisions,” *Nuclear Physics A*, **757**, pp. 102–183, 2005.
- [2] K. Adcox et al. (PHENIX Collaboration), “Formation of dense partonic matter in relativistic nucleus–nucleus collisions at RHIC: Experimental evaluation by the PHENIX Collaboration,” *Nuclear Physics A*, **757**, pp. 184–283, 2005.
- [3] J. F. Grosse-Oetringhaus for the ALICE Collaboration, “Overview of ALICE results at Quark Matter 2014,” *Nuclear Physics A*, **931**, pp. 22–31, 2014.
- [4] A.M. Sirunyan et al. (CMS Collaboration), “Event shape variables measured using multijet final states in proton-proton collisions at $\sqrt{s} = 13$ TeV,” *Journal of High Energy Physics*, vol. 2018, no. 12, article 117, 2018.
- [5] B. Abelev et al. (ALICE Collaboration), “Multiplicity dependence of two-particle azimuthal correlations in pp collisions at the LHC,” *Journal of High Energy Physics*, vol. 2013, no. 9, article 49, 2013.
- [6] T. Mizoguchi, M. Biyajima, N. Suzuki, “Analyses of whole transverse momentum distributions in $p\bar{p}$ and pp collisions by using a modified version of Hagedorn’s formula,” *International Journal of Modern Physics A*, vol. 32, article 1750057, 2017.
- [7] F.-H. Liu, Y.-Q. Gao, T. Tian, and B.-C. Li, “Unified description of transverse momentum spectrums contributed by soft and hard processes in high-energy nuclear collisions,” *The European Physical Journal A*, vol. 50, article 94, 2014.
- [8] R. Hagedorn, “Multiplicities, p_T distributions and the expected hadron \rightarrow quark-gluon phase transition,” *La Rivista del Nuovo Cimento*, vol. 6, no. 10, pp. 1–50, 1983.
- [9] E. K. G. Sarkisyan and A. S. Sakharov, “Multihadron production features in different reactions,” *AIP Conference Proceedings*, vol. 828, pp. 35–41, 2006.
- [10] E. K. G. Sarkisyan and A. S. Sakharov, “Relating multihadron production in hadronic and nuclear collisions,” *The European Physical Journal C*, vol. 70, pp. 533–541, 2010.
- [11] A. N. Mishra, R. Sahoo, E. K. G. Sarkisyan, and A. S. Sakharov, “Effective-energy budget in multiparticle production in nuclear collisions,” *The European Physical Journal C*, vol. 74, article 3147, 2014.
- [12] E. K. G. Sarkisyan, A. N. Mishra, R. Sahoo, and A. S. Sakharov, “Multihadron production dynamics exploring the energy balance in hadronic and nuclear collisions,” *Physical Review D*, vol. 93, article 054046, 2016.
- [13] E. K. G. Sarkisyan, A. N. Mishra, R. Sahoo, and A. S. Sakharov, “Centrality dependence of midrapidity density from GeV to TeV heavy-ion collisions in the effective-energy universality picture of hadroproduction,” *Physical Review D*, vol. 94, article 011501(R), 2016.
- [14] E. K. G. Sarkisyan, A. N. Mishra, R. Sahoo, and A. S. Sakharov, “Effective-energy universality approach describing total multiplicity centrality dependence in heavy-ion collisions,” *EPL*, vol. 127, article 62001, 2019.
- [15] A. N. Mishra, A. Ortiz, and G. Paić, “Intriguing similarities of high- p_T particle production between pp and A - A collisions,” *Physical Review C*, vol. 99, article 034911, 2019.
- [16] S. Chatrchyan et al. (CMS Collaboration), “Study of the inclusive production of charged pions, kaons, and protons in pp collisions at $\sqrt{s} = 0.9, 2.76,$ and 7 TeV,” *The European Physical Journal C*, vol. 72, article 2164, 2012.
- [17] P.-P. Yang, F.-H. Liu, R. Sahoo, “A new description of transverse momentum spectra of identified particles produced in proton-proton collisions at high energies,” *Advances in High Energy Physics*, vol. 2020, article 6742578, 2020.
- [18] C. Tsallis, Z. G. Arenas, “Nonextensive statistical mechanics and high energy physics,” *EPJ Web of Conferences*, vol. 71, article 00132, 2014.
- [19] L. Adamczyk et al. (STAR Collaboration), “Jet-hadron correlations in $\sqrt{s_{NN}} = 200$ GeV p+p and central Au+Au collisions,” *Physics Review Letters*, vol. 112, article 122301, 2014.
- [20] J. Kapitán for the STAR Collaboration, “Jets in 200 GeV p+p and d+Au collisions from the STAR experiment at RHIC,” *Journal of Physics: Conference Series*, vol. 270, article 012015, 2011.
- [21] J. Adam et al. (STAR Collaboration), “Longitudinal double-spin asymmetries for dijet production at intermediate pseudorapidity in polarized pp collisions at $\sqrt{s} = 200$ GeV,” *Physical Review D*, vol. 98, article 032011, 2018.
- [22] M. Cacciari, G. P. Salam, G. Soyez, “The anti- k_t jet clustering algorithm,” *Journal of High Energy Physics*, vol. 2008, no. 4, article 63, 2008.
- [23] J. Adam et al. (ALICE Collaboration), “Centrality dependence of charged jet production in p-Pb collisions at $\sqrt{s_{NN}} = 5.02$ TeV,” *The European Physical Journal C*, vol. 76, article 271, 2016.
- [24] B. Abelev et al. (ALICE Collaboration), “Measurement of charged jet suppression in Pb-Pb collisions at $\sqrt{s_{NN}} = 2.76$ TeV,” *Journal of High Energy Physics*, vol. 2014, no. 3, article 13, 2014.
- [25] V. M. Abazov et al. (D0 Collaboration), “Measurement of the ratio of differential cross sections $\sigma(p\bar{p} \rightarrow Z + b\text{jet})/\sigma(p\bar{p} \rightarrow Z + \text{jet})$ in $p\bar{p}$ collisions at $\sqrt{s} = 1.96$ TeV,” *Physical Review D*, vol. 87, article 092010, 2013.

- [26] V. M. Abazov et al. (D0 Collaboration), “Studies of W boson plus jets production in $p\bar{p}$ collisions at $\sqrt{s} = 1.96$ TeV,” *Physics Review D*, vol. 88, article 092001, 2013.
- [27] S. Chatrchyan et al. (CMS Collaboration), “Measurement of jet multiplicity distributions in $t\bar{t}$ production in pp collisions at $\sqrt{s} = 7$ TeV,” *The European Physical Journal C*, vol. 74, article 3014, 2014.
- [28] G. Aad et al. (ATLAS Collaboration), “Measurement of jet shapes in top-quark pair events at $\sqrt{s} = 7$ TeV using the ATLAS detector,” *The European Physical Journal C*, vol. 73, article 2676, 2013.
- [29] G. Aad et al. (ATLAS Collaboration), “Measurements of normalized differential cross sections for $t\bar{t}$ production in pp collisions at $\sqrt{s} = 7$ TeV using the ATLAS detector,” *Physics Review D*, vol. 90, article 072004, 2014.
- [30] G. Aad et al. (ATLAS Collaboration), “Search for $t\bar{t}$ resonances in the lepton plus jets final state with ATLAS using 4.7 fb^{-1} of pp collisions at $\sqrt{s} = 7$ TeV,” *Physics Review D*, vol. 88, article 012004, 2013.
- [31] D. Benjamin for the ATLAS Collaboration, “A search for $t\bar{t}$ resonances in the lepton plus jets final state with ATLAS using 14 fb^{-1} of pp collisions at $\sqrt{s} = 8$ TeV,” EPJ Web of Conferences, vol. 60, article 20044, 2013.
- [32] G. Aad et al. (ATLAS Collaboration), “Measurement of the $t\bar{t}$ production cross-section as a function of jet multiplicity and jet transverse momentum in 7 TeV proton-proton collisions with the ATLAS detector,” *Journal of High Energy Physics*, vol. 2015, no. 1, article 20, 2015.
- [33] S. Chatrchyan et al. (CMS Collaboration), “Measurement of the production cross sections for a Z boson and one or more b jets in pp collisions at $\sqrt{s}=7$ TeV,” *Journal of High Energy Physics*, vol. 2014, no. 6, article 120, 2014.
- [34] CMS Collaboration, “Search for pair production of resonances decaying to a top quark plus a jet in final states with two leptons,” CERN Document Server – CMS Physics Analysis Summaries: CMS-PAS-B2G-12-008, 2012, <https://cds.cern.ch/record/1630845/>
- [35] G. Aad et al. (ATLAS Collaboration), “Measurement of the electroweak production of dijets in association with a Z-boson and distributions sensitive to vector boson fusion in proton-proton collisions at $\sqrt{s} = 8$ TeV using the ATLAS detector,” *Journal of High Energy Physics*, vol. 2014, no. 4, article 31, 2014.
- [36] M. Aaboud et al. (ATLAS Collaboration), “Search for heavy particles decaying into top-quark pairs using lepton-plus-jets events in proton-proton collisions at $\sqrt{s} = 13$ TeV with the ATLAS detector,” *The European Physical Journal C*, vol. 78, article 565, 2018.
- [37] M. Aaboud et al. (ATLAS Collaboration), “Measurement of the cross-section for electroweak production of dijets in association with a Z boson in pp collisions at $\sqrt{s} = 13$ TeV with the ATLAS detector,” *Physics Letters B*, vol 775, pp. 206–228, 2017.
- [38] ATLAS Collaboration, “Measurement of the $t\bar{t}$ production cross-section in the lepton+jets channel at $\sqrt{s} = 13$ TeV with the ATLAS experiment,” CERN Document Server – ATLAS Note: ATLAS-CONF-2019-044, 2019, <https://cds.cern.ch/record/2690717/>
- [39] W. Busza, K. Rajagopal, W. van der Schee, “Heavy ion collisions: The big picture and the big questions,” *Annual Review of Nuclear and Particle Science*, vol. 68, pp. 339–376, 2018
- [40] M. Aaboud et al. (ATLAS Collaboration), “Measurement of the nuclear modification factor for inclusive jets in Pb+Pb collisions at $\sqrt{s_{NN}} = 5.02$ TeV with the ATLAS detector,” *Physics Letters B*, vol. 790, pp. 108–128, 2019.
- [41] H.-L. Lao, F.-H. Liu, R. A. Lacey, “Extracting kinetic freeze-out temperature and radial flow velocity from an improved Tsallis distribution,” *The European Physical Journal A*, vol. 53, article 44, 2017.